Biosensors and Bioelectronics 116 (2018) 108–115

Contents lists available at ScienceDirect

Biosensors and Bioelectronics

journal homepage: www.elsevier.com/locate/bios

# Ultrasensitive dual probe immunosensor for the monitoring of nicotine induced-brain derived neurotrophic factor released from cancer cells

Mahmood H. Akhtar[a], Khalil K. Hussain[a], N.G. Gurudatt[a], Pranjal Chandra[a,b], Yoon-Bo Shim[a,*]

[a] Department of Chemistry and Institute of BioPhysio Sensor Technology (IBST), Pusan National University, Busan 46241, South Korea
[b] Department of Biosciences and Bioengineering, Indian Institute of Technology Guwahati, Guwahati 781039, Assam, India

ARTICLE INFO

*Keywords:*
Immunosensor
Neurotrophins
Brain-derived neurotrophic factor
Dual probe sensor
Bioconjugate particles

ABSTRACT

Brain-derived neurotrophic factor (BDNF) was detected in the extracellular matrix of neuronal cells using a dual probe immunosensor (DPI), where one of them was used as a working and another bioconjugate loading probe. The working probe was fabricated by covalently immobilizing capture anti-BDNF (Cap Ab) on the gold nanoparticles (AuNPs)/conducting polymer composite layer. The bioconjugate probe was modified by drop casting a bioconjugate particles composed of conducting polymer self-assembled AuNPs, immobilized with detection anti-BDNF (Det Ab) and toluidine blue O (TBO). Each sensor layer was characterized using the surface analysis and electrochemical methods. Two modified probes were precisely faced each other to form a microfluidic channel structure and the gap between inside modified surfaces was about 19 μm. At optimized conditions, the DPI showed a linear dynamic range from 4.0 to 600.0 pg/ml with a detection limit of 1.5 ± 0.012 pg/ml. Interference effect of IgG, arginine, glutamine, serine, albumin, and fibrinogene were examined and stability of the developed biosensor was also investigated. The reliability of the DPI sensor was evaluated by monitoring the extracellular release of BDNF using exogenic activators (ethanol, $K^+$, and nicotine) in neuronal and non-neuronal cells. In addition, the effect of nicotine onto neuroblastoma cancer cells (SH-SY5Y) was studied in detail.

## 1. Introduction

Neurotrophins (NTs), a family of small and structurally related signaling proteins, are responsible in the survival, growth, and development of the mammalian nervous system. Various types of NTs have been discovered, such as nerve growth factor (NGF), neurotrophin-3 (NT-3), brain-derived neurotrophic factor (BDNF), and NT-4/5 (Nagahara et al., 2011). Among them, BDNF has been widely studied and known to be expressed in the central and peripheral nervous systems through ligation with tropomyosin receptor kinase B (TrKB). The regulated synthesis and secretion of BDNF plays an important role in learning and memory, neuronal growth, and synaptic transmission as well as plasticity of neurotransmitters (Su et al., 2014; Nagahara et al., 2011; Egan et al., 2003). Several biological, pharmacological, and genetic studies have suggested that BDNF is one of the significant factors involves in the major neurological and psychiatric disorders, such as Parkinson's, Alzheimer's, Huntington's, amyotrophic lateral sclerosis, stroke, bipolar disorder, depression, and stress (Novartis Foundation, 2008; Suzuki et al., 2014). Interestingly, it has also been reported that the level of BDNF increases under the external stimulators, such as $K^+$, nicotine, and alcohol (Balkowiec et al., 2000; Serres et al., 2006; Gärtner et al., 2002). Of them, nicotine is one of the most widely abused addictive alkaloids and has been shown to produce some roles in neurodegenerative disorders. Thus, the study of secretory BDNF level in the presence of these stimuli especially nicotine would be significant in clinical, pharmaceutical, and biomedical fields thereby opening wide range of applications like drug screening, therapeutics, and clinical treatments.

So far, BDNF has been analyzed in various neuronal cells with the developed techniques employing enzyme-linked immunosorbent assay (ELISA) (Lever et al., 2001; Elfving et al., 2010), electrochemiluminescence (Newton et al., 2005), fluorescence (Nakajima et al., 2008), or high-performance liquid chromatography (HPLC) (Lyons et al., 1999). These techniques are useful, however, they are time consuming, requiring large sample volumes and lacks of miniaturization for onsite analysis. On the other hand, electrochemical methods are considered valuable and promising ones due to their robustness, cost-effectiveness, and miniaturization ability (Hussain et al., 2017). To date, electrochemical immunosensors have been developed on single electrode system and investigated towards their target molecules (Ronkainen et al., 2010; Hussain et al., 2016; Chikkaveeraiah et al., 2012). However, they may suffer from the low sensitivity due to

* Corresponding author.
*E-mail address:* ybshim@pusan.ac.kr (Y.-B. Shim).

https://doi.org/10.1016/j.bios.2018.05.049
Received 13 April 2018; Received in revised form 22 May 2018; Accepted 27 May 2018
Available online 28 May 2018
0956-5663/ 

the lack of effective immobilizations of mediators/catalysts and bioconjugate together on a single electrode, and most importantly, they cannot be translated for *in vivo* application. To overcome these issue, one of the possible way is to immobilize the indicator molecule onto the second electrode; thereby formation of immune complex occurs without external incubation. Thus, the fabrication of DPI comprising of a nano-bioconjugate/catalysts on one probe and reaction antibody immobilized onto other probe containing mediator surface would be an effective analytical approach for *in vitro* as well as *in vivo* applications. Such immunosensors containing the nano-bioconjugate particles and antibody onto two different probes have not been reported to date. Therefore, we developed an amperometric immunosensor in a microfluidic architecture using dual probe assembly to detect BDNF and evaluated for the exogenic effect of nicotine on BDNF secretion from nerve cells for the first time.

To fabricate a robust electrochemical biosensor, it is crucial to stably immobilize biomaterials on a sensor surface. Using functionalized conducting polymer (CP) formed on the probe surface is one of the excellent ways for stable sensor fabrication (Lee et al., 2001; Moon et al., 2017; Skotheim and Reynolds, 2007). However, only CP layer may not be able to enhance the electron transfer during the electrocatalytic process due to the lack of enough conductivity, therefore, incorporating CP with gold nanoparticles (AuNPs) is considered to be the most preferred way to enhance sensitivity, catalytic activity, structural integrity, and better conductivity (Naveen et al., 2017; Saha et al., 2012). Thus, polyterthiophene based CP [2,2:5,2-terthiophene-3-(p-benzoic acid)](pTTBA) containing (–COOH) group was electropolymerized onto AuNPs modified surface, where the stable immobilization of the antibody on the sensor surface was achieved through the amide bond formation between amine groups of antibody and –COOH groups of CP.

For signal generation in immunoreactions, different types of indicators have been used for sensing devices to generate a fluorescence (Qiu et al., 2017), photoelectrochemical (Lin et al., 2017; Zhang et al., 2018) or an electrochemical signal (Hermanson, 2013; Zhou et al., 2018). In case of most electrochemical immunosensors, bioconjugate is composed of enzyme or hydrazine to generate the signal, which limit the lifetime of the sensor system. Hence, it is worth to explore a stable molecules for electrochemical signal generation. One of the candidate is toluidine blue O (TBO), which is small, stable, inexpensive molecule and can be used as a redox indicator in electrochemical sensing without adding additional molecule like $H_2O_2$ to generate the electrochemical signal. Therefore, TBO can be one of ideal substitutes for enzymes in the synthesis of bioconjugate.

In the present study, a microfluidic immunosensor comprising of a pair of screen printed carbon electrodes (SPCE) has been developed to detect BDNF. The working probe was fabricated by covalently immobilizing capture anti-BDNF (Cap Ab) on the AuNPs/CP composite layer. The bioconjugate loading probe (bioconjugate probe) was fabricated by drop casting of the bioconjugate particles composed of detection anti-BDNF (Det Ab) and TBO immobilized on self-assembled 4′-([2,2′:5′,2"-terthiophen]-3′-yl)-[1,1′-biphenyl]-4-carboxylic acid (pTTBPA) at AuNPs. After the modification of both working and bioconjugate probes, they were precisely attached and wrapped. The detection mechanism is based on the microfluidic sandwiched approach, where the bioconjugate particles are readily available onto the bioconjugate probe for signal generation. Therefore, making the detection method simpler compared to the conventional immunosensor approaches, which require additional incubation steps. Effect of various exogenous activators (ethanol, $K^+$, and nicotine) on the release of BDNF from various cancer cells was also studied to show the prospective importance of sensing system in drug screening and therapeutics. Moreover, the effect of nicotine on the induced-release of BDNF from neuroblastoma cancer cells (SH-SY5Y) was confirmed using the proposed sensor in terms of time and concentrations profiles.

## 2. Experimental

### 2.1. Reagents

Lyophilized BDNF antibody (Cap Ab and Det Ab) were purchased from Thermo Fisher Scientific. Lyophilized BDNF (expressed in *E. coli, 27* kDa), TBO, sodium phosphate dibasic, sodium phosphate monobasic, RPMI-1640 medium, bovine serum albumin (BSA), trypsin-ethylenediaminetetraacetic acid (EDTA), penicillin/streptomycin, PBS solution, 1-ethyl-3-[3-(dimethylamino)propyl]-carbodiimide (EDC), N-hydroxysuccinimide ester (NHS), gold(III) chloride trihydrate ($HAuCl_4$), trisodium citrate, sulfuric acid ($H_2SO_4$), sodium chloride, hydrogen peroxide ($H_2O_2$, 30 wt% in water), di (propylene glycol) ethyl ether, tri (propylene glycol) ethyl, and phosphate-buffered saline (PBS) solution were purchased from Sigma-Aldrich (USA) and used as received. Cancer cell lines SH-SY5Y, PC-12, and noncancerous Vero cell lines were purchased from the American Type Culture Collection (USA). Monomer, [2,2:5,2-terthiophene-3-(p-benzoic acid)](pTTBA) bearing a carboxylic acid group, was synthesized according to the previous report (Kim et al., 2012).

### 2.2. Instruments

The electrochemical experiments were performed using an all-in-one screen-printed carbon electrode (SPCE), consist of working, reference (Ag/AgCl), and counter electrodes, respectively. Kosentech PT-1 model and an EG & G PAR 273A model galvanostat was used to Cyclic voltammetry (CV) and chronoamperometry. The impedance spectra were obtained with the EG&G Princeton Applied Research, PARSTAT 2630 multimode. An AFM device developed by Veeco metrology and equipped with a Nanoscope IV controller (Veeco), was used to take the AFM images of the fabricated sensor probe. XPS experiments were performed in KBSI (Busan) using a VG Scientific ESCA Lab 250 XPS spectrometer coupled with a monochromatic Al Kα source with charge compensation and XPSPEAK41 software was used to analyze the XPS data. QCM experiments were performed at an Au-coated working electrode (area: 0.196 $cm^2$; 9.0 MHz; ATcut quartz crystal) using a SEIKO EG&G model QCA 917 and a PAR model 263A potentiostat/galvanostat (USA).

### 2.3. Preparation of bioconjugate particles

Bioconjugate particles were prepared by immobilizing Det Ab and TBO chemically attached using EDC/NHS onto a self-assembled pTTBPA at AuNPs. To do this, SAM of pTTBPA and AuNPs composite were synthesized using the previously reported method (Zhu et al., 2012). At first, 50 ml of $HAuCl_4$ (0.01 wt%) was dissolved in $H_2O$ and mixed with 1 ml of 38.8 mM trisodium citrate. After 1 min, 0.5 ml of $NaBH_4$ (0.1 M) solution was added drop wise under gentle stirring. The color of resulting solution turned to pink violet upon adding $NaBH_4$, which showed the formation of AuNPs. Next, the pTTBPA was self-assembled onto the AuNPs 1:1 ratio (*v/v*) by mixing 1 ml of pTTBPA (1 mM) and incubating the reaction solution for 12 h, followed by successive centrifugation and washing steps. The pTTBPA at AuNPs was obtained in the final step (Koh et al., 2011) and was treated with 10 mM of EDC/NHS for 6 h to activate the –COOH groups of pTTBPA. Finally, 1 ml of the self-assembled monolayer (SAM) was mixed with 0.2 ml Det Ab and 0.2 ml of TBO (0.5 mM) and incubated for 12 h at 4 °C (optimized). After incubation, the solution mixture was centrifuged and washed with 0.1 M PBS to remove the unbound Det Ab and/or TBO. Finally, the designed bioconjugate particles (Det Ab/ TBO-SAM) was stored at 4 °C until further use

### 2.4. Fabrication of working and bioconjugate probes

At first, working probe was prepared by rinsing the SPCE with water followed by electrodeposition of AuNPs using LSV (Fig. S1(a)). Prior to make the layer of CP on SPCE/AuNPs surface, 1.0 mM monomer (2,2:5,2-terthiophene-3-(p-benzoic acid)) was prepared in a mixture solution of di(propylene glycol) ethyl ether and tri(propylene glycol) ethyl ether (1:1 vol ratio, 5 ml). Afterward, conducting polymer (CP), pTTBA was electropolymerized by cycling the potential twice from 0.0 to + 1.4 V (*vs.* Ag/AgCl) at 100 mV $s^{-1}$ employing CV (Fig. S1 (b)), followed by rinsing the polymerized surface with PBS to remove any excess of monomer. Next, the SPCE/AuNPs/CP surface was immersed in 10 mM EDC/NHS solution for 6 h to activate the –COOH groups of pTTBA. After activation, an appropriate amount (optimized) of Cap Ab (5 µl) was drop casted on the probe surface and kept for 6 h at 4 °C in moist condition to immobilize the Cap Ab forming SPCE/AuNPs/CP-Cap Ab as the final working probe. In the next step, 2% bovine serum albumin (BSA) prepared in a 0.01 mM PBS medium was used for 1.0 h to block the unreacted sites at the probe surface to reduce the false positive results. The bioconjugate probe was modified by simply drop casting the bioconjugate particles on the SPCE and allowed to dry under ambient laboratory conditions. After the modification of both working and bioconjugate probes, they were precisely attached, wrapped, and named as dual immunosensor probe (DPI). The Real photograph of the DPI sensor is shown in (Fig. S2), where (a) represent working probe, (b) bioconjugate probe before assembly, and (c) after assembly.

### 2.5. Preparation of cancer cells sample

The neuronal (SH-SY5Y, PC-12) cell lines were selected, because they provide suitable model for studying neuronal mechanisms and demonstrate an excellent activity of BDNF-TrkB signaling (Serres et al., 2006; Canossa et al., 1997), whereas non-neuronal (Vero) cell line was used to validate our results. Neuronal and non-neuronal cell lines were maintained in T75 cell culture flasks containing RPMI-1640 medium supplemented with 10% fetal bovine serum (FBS) and 100 units/ml of penicillin/streptomycin (Gibco). The cells were maintained in an incubator at 37 °C in a 95% humidified atmosphere and 5% carbon dioxide. The cells were passaged every 5–6 days and medium was replaced every two days until 95% confluency was obtained and then subcultured. Before every experiment, cells were suspended in sterile PBS and enumerated using a disposable C-Chip (South Korea) to confirm the reproducibility and accuracy of the results. For different stimuli treatments, 1 ml of cell suspension was obtained and poured into wells of 24 well plates and allowed to incubate for 24 h. Subsequently, the cells were removed from culture conditions following trypsinization and suspended in 0.1 M PBS (pH 7.5) and examined the exogenic effects of alcohol, $K^+$, and nicotine on BDNF expression.

### 2.6. Electrochemical measurement procedure

After the fabrication of the DPI, the analytical performance was investigated using various electrochemical methods. Cyclic voltammetry was performed in 0.1 M PBS (pH 7.4) and the potential was scanned from + 0.0 and − 0.6 V at a scan rate of 50.0 mV $s^{-1}$. Under optimized conditions, chronoamperometric experiments were carried out at applied potential of − 0.35 V *vs.* Ag/AgCl using different concentrations of BDNF.

## 3. Results and discussion

The DPI was fabricated using two SPCEs, where each SPCE was composed of 20 mm and 5 mm in length and width, respectively. After modifying both the SPCEs (working and bioconjugate probes), they were assembled as their modified surface faced each other with an optimized gap of 19 µm, creating a 10 mm long microfluidic channel with one inlet and two outlets. The mechanism of detection is based on the sandwich immunosensing approach, where the signal was generated by the redox indicator TBO. At first, the measuring solution enters into the optimized DPI gap due to the capillary force action, through this step anti-body-antigen complex is formed onto the working probe. Thereafter, similar reaction occurs between antigen and Det Ab covalently attached on the bioconjugate particles consequently, the bioconjugate detached from the bioconjugate probe in the measuring solution between two probes. The detachment of bioconjugate is due to the weak physio adsorption of the bioconjugate onto bioconjugate probe and immune reaction between Det Ab and BDNF. The sensor design, components, and the detection principle are shown in Scheme 1.

### 3.1. Characterization of the immunosensor probe

We characterized the probe surfaces using XPS, after taken 50 s of Ar ion gas etching and calibrated with a C1s peak at 284.6 eV as an

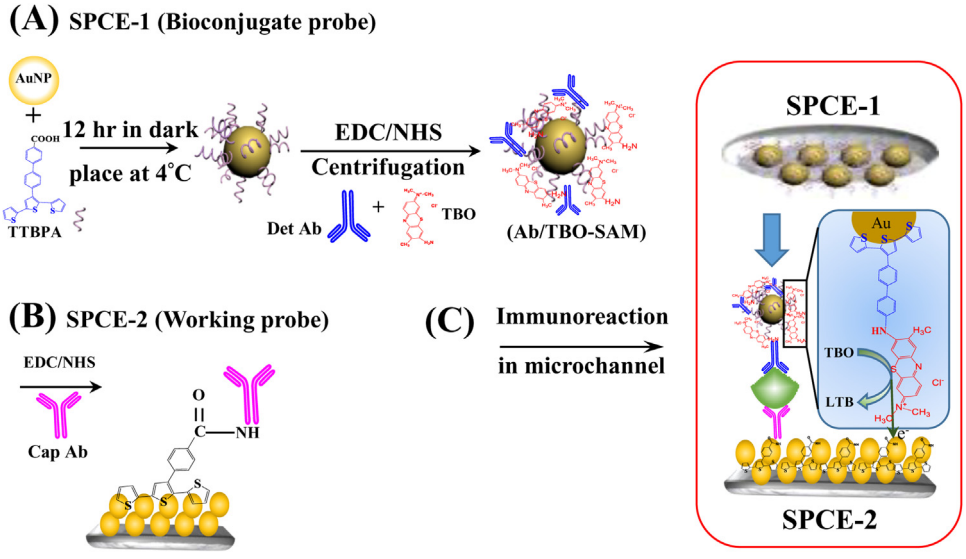


**Scheme 1.** Schematic representation of the fabrication steps of (A) working probe, (B) bioconjugate probe, and (C) detachment of bioconjugate particles and immunoreaction in microchannel structure.

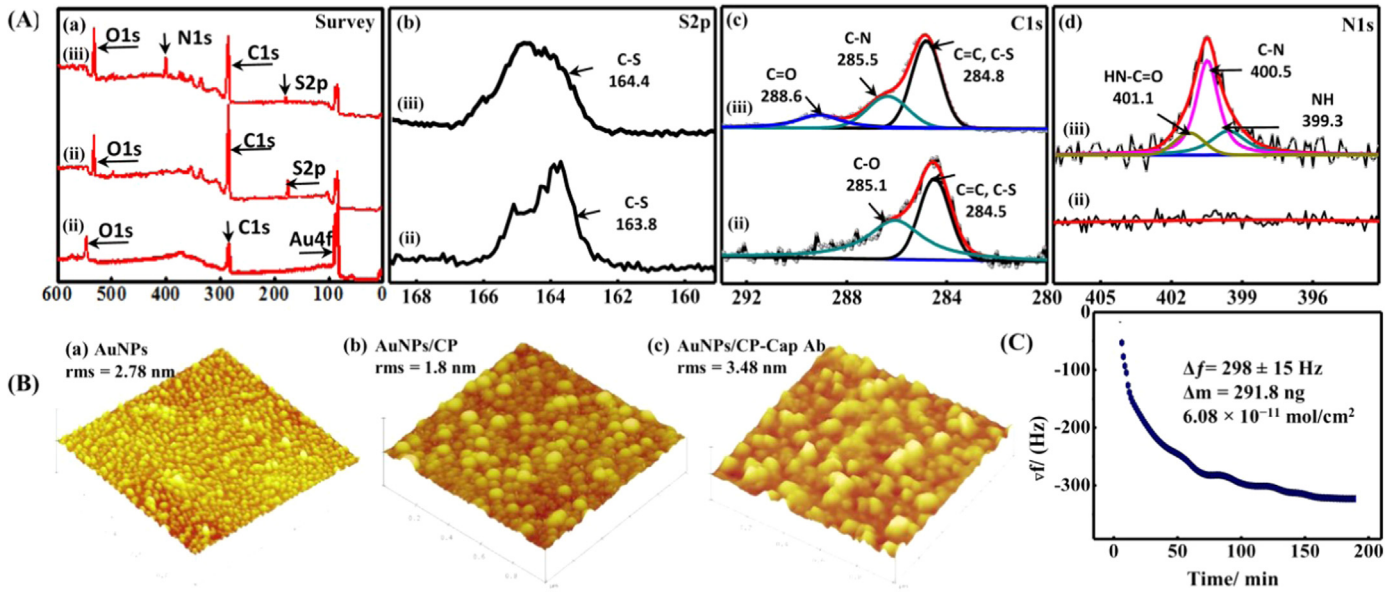


**Fig. 1.** (A) (a) XPS survey spectra and (b, c, d) deconvoluted peaks of S2p, C1s, and N1s, respectively for (ii) AuNPs/CP and (iii) AuNPs/CP-Cap Ab (B) AFM images of (i) AuNPs, (ii) AuNPs/CP, and (iii) AuNPs/CP-Cap Ab. (C) QCM response for real time immobilization of antibody (Cap Ab) onto AuNPs/CP modified surface.

internal standard. The survey spectra for each layer of the sensor probe are shown in Fig. 1(A-a), and the deconvoluted peaks for S2p (b), C1s (b), and N1s (d) have been discussed as follows. The Au4f spectrum of SPCE/AuNPs shows two clear peaks at 85.7 and 82.4 eV, which appeared due to the AuNPs deposition (Fig. S3). The S2p spectrum for the SPCE/AuNPs/CP surface (i) clearly shows a peak at 163.8 due to the C–S bond present in the CP, indicating the formation of the nanocomposite film. The peak at 163.8 is not observed for SPCE/AuNPs, indicating that the peak in the earlier case is merely due to the electropolymerization of CP onto the SPCE/AuNPs surface. The deconvoluted spectra of C1s for SPCE/AuNPs/CP are shown in Fig. 1(A (c-ii)), indicating two distinct peaks at 284.5 and 285.1 eV that are corresponded to C-C/C=C, C–S, and C–O bonds, respectively. After immobilization of the Cap Ab onto the SPCE/AuNPs/CP surface, the peak shift in the C1s and the presence of N1s are observed. An additional peak appears at 285.5 eV corresponding to C–N bond formation between –COOH groups of CP and $–NH_2$ groups of Cap Ab, and the C-C/C-S peak is shifted toward a higher binding energy at 284.8 eV as shown in Fig. 1(A (c-iii)). The deconvoluted N1s spectrum for SPCE/AuNPs/CP-Cap Ab surface shows three clear peaks at 399.3, 400.5, and 401.6 eV, corresponding to the –NH, C–N, and HN-C=O bonds, respectively due to the covalent bonding between $–NH_2$ groups of Cap Ab and –COOH groups of CP showing successful immobilization of the Cap Ab. These peaks were not observed when SPCE/AuNPs/CP surface was examined, indicating that the peaks arose merely due to the Cap Ab immobilization. Further, the surface of the sensor probe (SPCE/AuNPs/CP-Cap Ab) were characterized by AFM using highly oriented pyrolytic graphite (HOPG) electrode as shown in Fig. 1(B). The images reveal clearly the electrodeposited AuNPs having the particle size of 25 ± 2 nm, which is also determined by the roughness factor and measured in root mean square (rms) value of 2.8 nm (Fig. 1(B-a)). A homogeneous layer of CP coated on the AuNPs surface with comparative low rms value of 1.8 nm is shown in Fig. 1(B-b), indicating that the AuNPs surface is effectively covered with the CP (Chandra et al., 2015). The Cap Ab treated layer exhibits rms value of 3.5 nm due to the immobilization of Cap Ab (Fig. 1(B-c)), indicating the successful immobilization of Cap Ab on the AuNPs/CP surface. Finally, QCM was also performed to confirm the Cap Ab immobilization, where the amount of Cap Ab was determined based on the frequency change (Fig. 1(C)). During Cap Ab immobilization, the frequency reaches a stable state after 150.0 ± 4.0 min with an overall frequency change ($\Delta f$) of 298 ± 15 Hz, corresponding to a mass change ($\Delta m$) of 291.8 ng ± 21.3 ng using Eq. (1).

$$\boldsymbol{\Delta m = \Delta f} \times 5.608(\mathrm{ng}/c\mathbf{m^2})/\mathrm{Hz} \times \mathbf{0.196\ cm^2} \quad (1)$$

where, $\Delta f$ was the change in frequency, 5.608 (ng/cm$^2$)/Hz was the sensitivity factor calculated from the physical constant for quartz, and 0.196 cm$^2$ was the probe area. The change in mass ($\Delta$m) was calculated to be 291.8 ng with the surface coverage of $6.08 \times 10^{-11}$ ng/cm$^2$. The results clearly show the immobilization of Cap Ab on SPCE/AuNPs/CP probe surface.

### 3.2. Detection of BDNF with the dual probe immunosensor

Prior to examine DPI, we confirmed the immunoreaction between BDNF and the single working probe (SPCE/AuNPs/CP-Cap Ab) using electrochemical impedance spectroscopy (EIS). For this purpose, the sensor probe was incubated with known concentration of BDNF for 20 min to form SPCE/AuNPs/CP-Cap Ab/BDNF. After washing, the EIS spectra in Nyquist plots were recorded in PBS as shown in Fig. 2(A). A sharp increase in the Rct value ($\Delta$Rct = 12.5 kΩ) was observed after the interaction between 10 ng/ml BDNF and the sensor probe. In order to confirm the stable and reproducible immunoreaction, the concentration depended-interaction was studied between 10 and 50 ng/ml, where the $\Delta$Rct value increased linearly with the increase in the BDNF concentration. A calibration plot was obtained having the linear equation as follows: $\Delta$Rct (kΩ) = 10.04 (± 0.487) + 0.281 (± 0.0147) [BDNF], with the correlation coefficient of 0.986 (Fig. 2(A)) (n = 5). The interaction of BDNF with SPCE/AuNPs/CP without Cap Ab was also tested, where no increase in the Rct was observed, indicating that the increase in the Rct value at the immunosensor surface was merely due to binding of BDNF with Cap Ab (data not shown).

Furthermore, to evaluate the ability of the DPI to detect BDNF using dual probes design, the device was allowed to react with BDNF for 20 min. Due to the capillary action, the sample solution containing BDNF was pulled into the flow channel, hence performing two functions; completing the immune reaction as well as detaching the bioconjugate particles from the bioconjugate probe. After binding and subsequent washing. Cyclic voltammetry (CV) was performed in a 0.1 M deoxygenated PBS by cycling the potential between + 0.0 and − 0.6 V at a scan rate of 50.0 mV s$^{-1}$. A redox peak was observed at − 265/ − 300 mV corresponding to the redox reaction of TBO itself

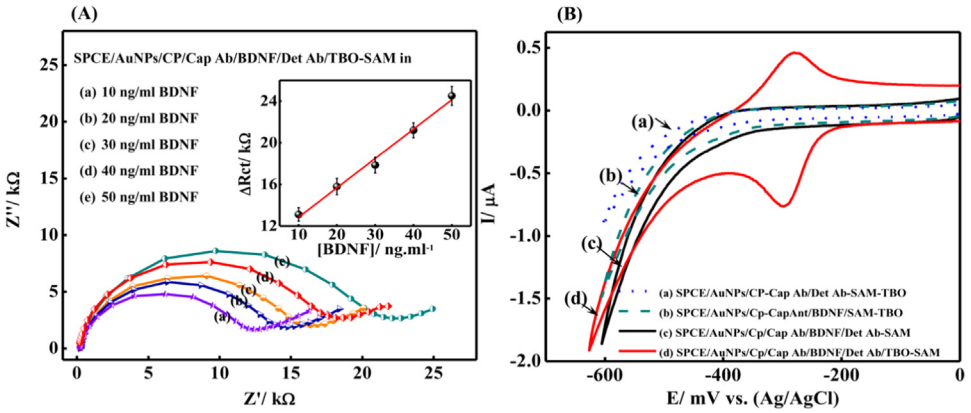


**Fig. 2.** (A) The obtained EIS signals recorded after BDNF interaction in a 0.1 M PBS (pH 7.4), where (inset) the linear plot for ΔRct increased when the higher concentration of BDNF interacted with SPCE/AuNPs/CP-Cap Ab sensor probe. (B) CVs recorded for the constructed DPI as a control experiment without BDNF at (a) DPI, without Ab at (b), and without TBO at (c).

(Fig. 2(B) (d)): red curve), which was directly proportional to the scan rate due to the surface-confined electrochemical reaction, indicating that BDNF was successfully sandwiched between the working probe and the bioconjugate particles (Fig. S4). To confirm that the redox peak at − 265/− 300 mV arose due the successful interaction of BDNF in the proposed scheme, we performed three control experiments. In the first control experiment, blank solution was passed (without BDNF) through the microchannel of DPI, interestingly no redox peak was observed at − 260/− 300 mV, indicating that bioconjugate particles could not bind to the SPCE/AuNPs/CP-Cap Ab surface (Fig. 2 (B)(a)). In the second control experiment, only SAM-TBO modified bioconjugate (without Det Ab) was drop casted on the bioconjugate probe and then combined with the working probe. Upon passing the solution containing BDNF, no redox peak was observed indicating that Det Ab is important to get the analytical signal (Fig. 2(B) (b)). In the final control experiment, the bioconjugate particles were prepared without TBO and drop casted on the bioconjugate probe to make DPI structure, similarly, no signal was observed when the solution containing BDNF was passed through the micro channel (Fig. 2(B) (c)). These results clearly indicate that the effective immune reaction of BDNF in the microenvironment is responsible for the redox peak of TBO attached onto the bioconjugate particles at − 265/− 300 mV. This also proves the successful formation of the bioconjugate and its importance in BDNF detection.

### 3.3. Optimization of the analytical parameters

The analytical parameters for the BDNF detection using the proposed immunosensor were optimized in terms of temperature, pH, Cap Ab concentration, and incubation time, where BDNF concentration was kept constant. At first, the effect of temperature on the DPI performance was studied over the range of 20–50 °C as shown in Fig. 3 (A). The maximum response current was observed at 35 °C, which remained unchanged until 40 °C. The signal response, however, decreased drastically over 45 °C, possibly due to thermal denaturation of the Anti-BDNF and/or BDNF. Thus, 35 °C was selected as the optimum temperature, which is comparable to the human body fluids and *in vitro* culture conditions, showing the importance of the immunosensor for real sample analysis. The influence of pH was investigated in the range from 5.0 to 8.0, and an increase in the response signal was obtained as the pH was increased, however, at pH 7.5 maximum signal was observed, which decreased with the increase in the pH of the buffer (Fig. 3(B)). Based on this, pH of 7.5 was applied in subsequent experiments. It is valuable to mention that the optimized pH is comparable to the pH of various body fluids. An adequate concentration of antibody was also investigated for the immune-complexation with antigen to attain the best sensor performance. As shown in Fig. 3(C), the sensor was evaluated by incubating in various concentrations of Cap Ab ranging from 100 to 450 μg/ml. The response current of the sensor increased as the concentration increased from 100 to 300 μg/ml, while over 300 μg/ml, no significant increase in the signal was observed due to saturation effect. Therefore, 300 μg/ml Cap Ab concentration was used for the subsequent experiments. The effect of immunoreaction time between Cap Ab and BDNF was examined and optimized between 5 and 35 min. The response signal increased with increase in the immunoreaction time upto 20 min, while over this time no significant increase in the signal was observed, indicating 20 min is the optimum time for the immunoreaction (Fig. 3(D)).

### 3.4. Analytical performance of immunosensor, selectivity, and stability

Under the optimized experimental conditions, the analytical performance of the DPI for the quantitative detection of BDNF was performed using chronoamperometry. Fig. 4(A) shows the chronoamperometric signals of the immunosensor at − 0.35 V *vs.* Ag/AgCl (optimized) in deoxygenated PBS for the different concentrations of BDNF. Chronoamperometry clearly shows the increase in the current response according to the increase in the BDNF level, indicating that the target molecule has been effectively detected by the immunosensor in a sandwich format. Based on the data, a calibration plot was obtained, showing a dynamic range from 4.0 and 600.0 pg/ml (Fig. 5(A)). The linear regression equation for BDNF detection is expressed as follows: *I*p (μA) = 0.061 ( ± 0.0027) + 0.00037 ( ± 0.00084) [BDNF] with the correlation coefficient of 0.996. The detection limit was determined to be 1.5 ± 0.012 pg/ml based on the standard deviation of six individual measurements of the blank (95% confidence level, $n = 5$).

The selectivity of immunosensor was demonstrated by testing the compounds that were present in the real sample matrix, such as arginine, glutamine, serine, albumin, IgG, and fibrinogene. All these interfering compounds were tested at the concentration of 100, 200, and 500 pg/ml. Fig. 4 (B) shows a comparative response of interfering chemical along with BDNF, where negligible signal is observed for non-target molecules compared to BDNF (data shown only for 500 pg/ml). This clearly indicates that the proposed immunosensor is highly selective and has no interference from other molecules. We also examined the immunosensor performance to detect target BDNF in the presence of interfering molecules in a mixed sample solution. The sensitivity of the detection in this case was 97.3 ± 4% ($n = 5$) compared when BDNF was detected alone, indicating its highly selective detection in the presence of non-target molecules. The reproducibility of the immunosensor showed the RSD < 5.3% ($n = 5$) and the sensor-to-sensor RSD was < 4.8% (Fig. S5(a)). The negligible deviation was most likely due to the variation in the immunosensor fabrication steps and handling errors. We also evaluated the stability of the immunosensor with respect to the storage time, where 92.5 ± 4% sensitivity was retained up to four weeks. The response decreased about 7.5 ± 1% after four weeks and then further decreased with time, indicating that the designed immunosensor is stable up to four weeks (Fig. S5(b)).

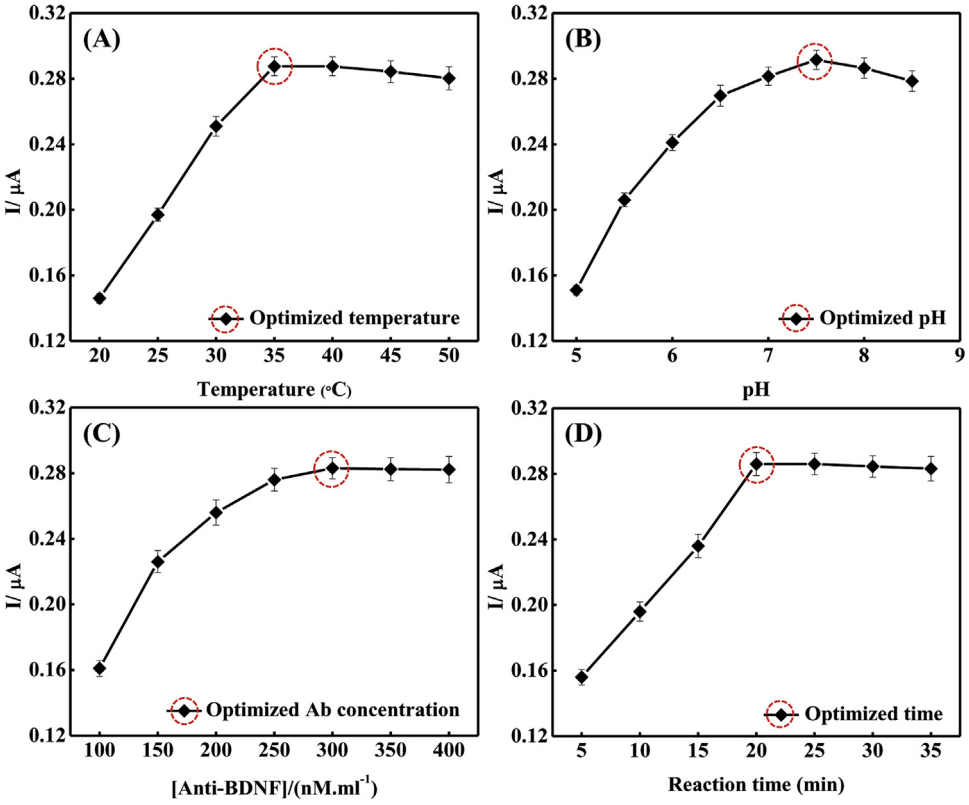


**Fig. 3. :** Optimization of the experimental parameters for the immunosensor (A) effect of temperature on the sensor performance. (B) optimum pH value for PBS buffer solution (C) adequate Cap Ab concentration, and (D) time required for Cap Ab/BDNF immune reaction.

### *3.5. Real samples analysis*

#### *3.5.1. Human serum analysis*

We detected BDNF in human serum samples to preliminary evaluate the reliability of sensor. For this, known concentrations (100, 200, and 300 pg/ml) of BDNF were spiked into whole serum and the recovery was estimated using the chronoamperometry at the designed immunosensor. The recovery was more than 98.1 ± 2.0% in all the cases, indicating that the proposed immunosensor is able to detect BDNF effectively in a real sample matrix. The calibration plot for BDNF detection showed the regression equation as follows: *Ip* (μA) = 0.054 (± 0.0032) + 0.00028 (± 0.00093) [BDNF] with the correlation coefficient of 0.996. The detection limit was determined to be 1.81 ± 0.012 pg/ml based on the standard deviation of five individual measurements of the blank (95% confidence level, $n = 5$). The detection limit in serum is slightly higher compared to the blank buffer, most likely due to the negligible interaction of the serum matrix components with the immunosensor surface.

#### *3.5.2. Nicotine induced-BDNF detection in cancer cells*

In addition to the human serum samples, the effect of exogenic activators on BDNF level in cultured cells was monitored. Therefore, we detected BDNF levels in neuronal cancer cells using SH-SY5Y and PC12 as model cell lines since these cells line are known to release BDNF in various cultural conditions (Stragier et al., 2015). Firstly, we tried to detect BDNF in SH-SY5Y cell line without adding any stimulant. In this case, negligible response signal was obtained indicating that the cells are releasing very low levels of BDNF as shown in Fig. 5 (A). Thereafter, we incubated these cells with alcohol, potassium ($K^+$), and nicotine which have been well known exogenic activators for BDNF release in extracellular matrix (Serres et al., 2006; Balkowiec et al., 2000). To do this, enumerated SH-SY5Y were treated with these exogenic activators

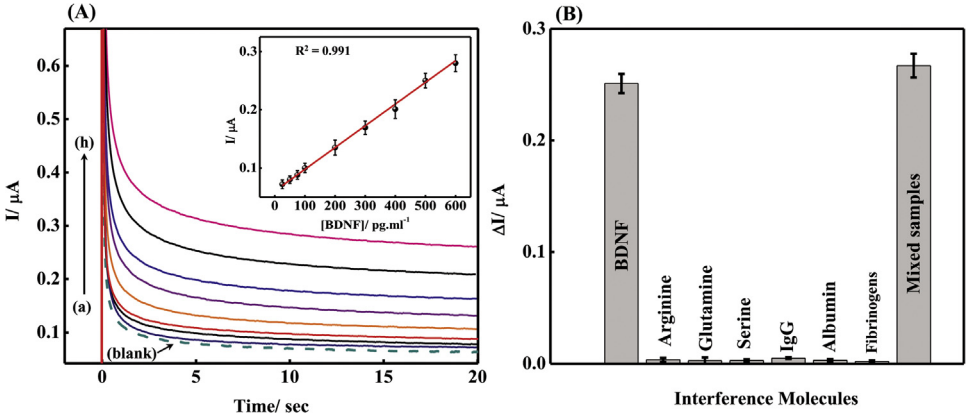


**Fig. 4.** (A) Chronoamperometric responses of the SPCE/AuNPs/CP-Cap Ab/BDNF/Det Ab/TBO-SAM immunosensor corresponding to the different concentrations of BDNF in PBS solution, and (inset) calibration plots showing the dynamic ranges from 4.0 to 600.0 pg/ml. (B) Interference response at the fabricated immunosensor in PBS (pH 7.5) containing potentially interfering molecules (glutamine arginine, serine, albumin, human IgG, and fibrinogene).

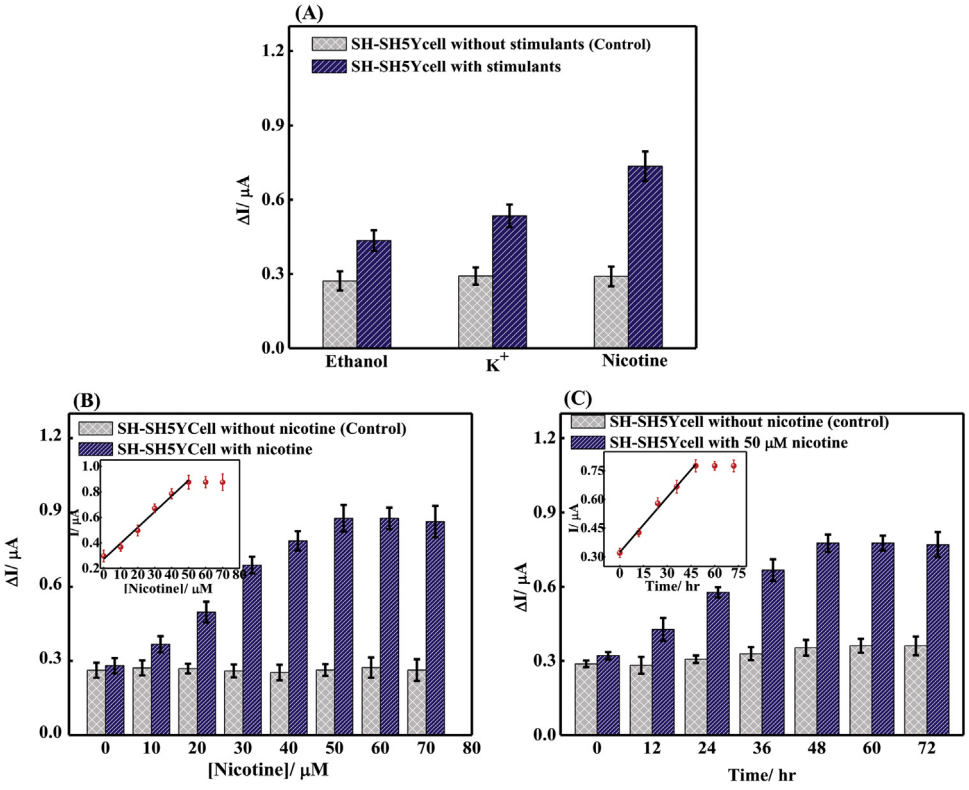


**Fig. 5.** (A) Effect of alcohol, potassium ($K^+$), and nicotine on the exogenic release of BDNF from SH-SY5Y cells. Effect of nicotine on the extracellular release of BDNF from SH-SY5Y cells in terms of (B) concentration and (C) time.

for 12 h in the separate experiment and after incubation, the extracellular matrix was determined for BDNF concentrations using the proposed immunosensor. It was interesting to observe in BDNF levels that three times higher signals were obtained in nicotine treated cells samples compared to the controls (activator untreated cells). Similar results were obtained when other two activators were treated, however, the signals in this case were slightly lower compared to that of nicotine treated cells (Fig. 5(A)). This is most likely due to the higher efficacy of nicotine as exogenic activator compared to ethanol and $K^+$, which adequately confirms the applicability of the proposed immunosensor to monitor the over-expression of BDNF due to the nicotine stimulations in neural cells. We also tested the effect of these exogenic activator for the release of BDNF using PC12 cell line. In this case, the signal response followed the similar trend, which was observed in the case of SH-SY5Y, indicating that the PC12 cells also released BDNF (Fig. S6).

We further extended our investigation towards time and dose dependent release of BDNF using exogenic activator in SH-SY5Y cell line. To do this, we selected nicotine as an exogenic activator, since the signal obtained using this molecule was highest compared to others (Fig. 5(A)). Firstly, enumerated cells were treated with nicotine at a concentration range between 0 and 70 μM for similar time span of time of 12 h. After processing the cell supernatant it was used to detect the BDNF levels. (Fig. 5(B)) shows the increase in signal from 0 to 50 μM nicotine concentration, while over 50 μM signal response remains constant. A calibration plot for dose dependent BDNF detection upon nicotine stimulation shows the regression equation as follows: *Ip* (μA) = 0.273 ( ± 0.0032) + 0.0128 ( ± 0.000093) [BDNF] with the correlation coefficient of 0.984, indicating the ability of BDNF detection using fabricated immunosensor in stimulatory conditions. Contrary to the nicotine treated cells, no substantial increase in the signal was observed for nicotine untreated cells. We also studied the effect of time of BDNF release using SH-SY5Y cells line where the concentration of nicotine was kept constant at 50 μM. The time-effect of nicotine on the exogenic release of BDNF was investigated between 1 and 72 h as shown in Fig. 5 (C). At 1 h negligible signal was observed, however, with increase in the time span from 5 to 48 h an increase in the signal was observed due to the extracellular release of BDNF. No signal was observed when cells were not treated with nicotine in this experimental setting, validating our results and clearly showing that the designed immunosensor is able to detect BDNF levels after treatment of exogenic activator in time dependent manner.

## 4. Conclusions

We report for the first time an electrochemical dual probe immunosensor in a microfluidic structure to detect BDNF in the extracellular matrix of nerve cells, where the exogenic effect of nicotine on BDNF secretion was evaluated. In addition, a new type of bioconjugate was fabricated, where the polymer precursor was self-assembled onto AuNPs followed by covalent attachment of Det Ab and TBO. The bioconjugate particles were drop casted onto the bioconjugate probe to reduce additional incubation steps, thereby making the detection mechanism more simple and fast. When the proposed DPI was exposed to the exogenously induced cell lines by cell activators (alcohol, $K^+$, and nicotine), it detected an increased extracellular level of BDNF and differentiated the neuronal from non-neuronal cells. Moreover, SH-S5Y5 cells demonstrated the maximum response due to the highest BDNF expression followed by PC-12 and Vero cells. The proposed sensing approach has numerous advantages over conventional electrochemical immunoassays such as fewer preparation steps, on site point of care device, and most importantly, the proposed method did not required an additional external incubation step for bioconjugate attachment as it is already available onto bioconjugate probe. Therefore, it can be applied for *in vivo* applications hence, the significance of this work is directly related to the clinical and pharmaceutical fields.

## Acknowledgement

This work was supported by the researcher program from National Research Foundation of Korea (NRF) grant funded by the Korea government (MSIP) (No, 2015R1A2A1A13027762).

## Appendix A. Supporting information

Supplementary data associated with this article can be found in the online version at http://dx.doi.org/10.1016/j.bios.2018.05.049.

## References

Balkowiec, A., Katz, D.M., 2000. J. Neurosci. 20, 7417–7423.
Canossa, M., Griesbeck, O., Berninger, B., Campana, G., Kolbeck, R., Thoenen, H., 1997. PNAS 94, 13279–13286.
Chandra, P., Noh, H.B., Pallela, R., Shim, Y.-B., 2015. Biosens. Bioelectron. 70, 418–425.
Chikkaveeraiah, B.V., Bhirde, A.A., Morgan, N.Y., Eden, H.S., Chen, X., 2012. ACS Nano 6, 6546–6561.
Elfving, B., Plougmann, P.H., Wegener, G., 2010. J. Neurosci. Methods 187 (1), 73–77.
Egan, M.F., Kojima, M., Callicott, J.H., Goldberg, T.E., Kolachana, B.S., Bertolino, A., Lu, B., 2003. Cell 112, 257–269.
Gärtner, A., Staiger, V., 2002. PNAS 99, 6386–6391.
Hermanson, G.T., 2013. Bioconjugate Techniques. Academic press.
Hussain, K.K., Gurudatt, N.G., Mir, T.A., Shim, Y.-B., 2016. Biosens. Bioelectron. 83, 312–318.
Hussain, K.K., Moon, J.M., Park, D.S., Shim, Y.B., 2017. Electroanalysis 29, 2190–2199.
Kim, D.M., Yoon, J.H., Won, M., Shim, Y.-B., 2012. Electrochim. Acta 67, 201–207.
Koh, W.C.A., Chandra, P., Kim, D.M., Shim, Y.B., 2011. Anal. Chem. 83 (16), 6177–6183.
Lee, T.Y., Shim, Y.-B., 2001. Anal. Chem. 73, 5629–5632.
Lever, I.J., Bradbury, E.J., Cunningham, J.R., Adelson, D.W., Jones, M.G., McMahon, S.B., Malcangio, 2001. J. Neurosci. 21, 4469–4477.
Lin, Y., Zhou, Q., Tang, D., Niessner, R., Knopp, D., 2017. Anal. Chem. 89 (10), 5637–5645.
Lyons, W.E., Mamounas, L.A., Ricaurte, G.A., Coppola, V., Reid, S.W., Bora, S.H., Tessarollo, L., 1999. PNAS 96, 15239–15244.
Moon, J.M., Kim, D.M., Kim, M.H., Han, J.Y., Jung, D.K., Shim, Y.-B., 2017. Biosens. Bioelectron. 91, 128–135.
Nagahara, A.H., Tuszynski, M.H., 2011. Nat. Rev. Drug Discov. 10, 209–219.
Nakajima, T., Sato, M., Akaza, N., Umezawa, Y., 2008. ACS Chem. Biol. 3, 352–358.
Naveen, M.H., Gurudatt, N.G., Shim, Y.B., 2017. Appl. Mater. Today 9, 419–433.
Newton, I.G., Forbes, M.E., Legault, C., Johnson, J.E., Brunso-Bechtold, J.K., Riddle, D.R., 2005. Neurobiol. Aging 26, 683–688.
Novartis Foundation, 2008. Growth Factors and Psychiatric Disorders. John Wiley & Sons, USA.
Qiu, Z., Shu, J., Tang, D., 2017. Anal. Chem. 89 (9), 5152–5160.
Ronkainen, N.J., Halsall, H.B., Heineman, W.R., 2010. Chem. Soc. Rev. 39, 1747–1763.
Saha, K., Agasti, S.S., Kim, C., Li, X., Rotello, V.M., 2012. Chem. Rev. 112, 2739–2779.
Serres, F., Carney, S.L., 2006. Brain Res. 1101, 36–42.
Skotheim, T.A., Reynolds, J. (Eds.), 2007. Handbook of Conducting Polymers, 2 Volume Set. CRC Press, Taylor & Francis Group, USA.
Stragier, E., Massart, R., Salery, M., Hamon, M., Geny, D., Martin, V., Lanfumey, L., 2015. Mol. Psychiatry 20, 405–412.
Su, B., Ji, Y.S., Sun, X.L., Liu, X.H., Chen, Z.Y., 2014. J. Biol. Chem. 289 (3), 1213–1226.
Suzuki, G., Tokuno, S., Nibuya, M., Ishida, T., Yamamoto, T., Mukai, Y., Mitani, K., Tsumatori, G., Scott, D., Shimizu, K., 2014. PLoS One 9 (2), e89455.
Zhang, K., Lv, S., Lin, Z., Li, M., Tang, D., 2018. Biosens. Bioelectron. 101, 159–166.
Zhu, Y., Chandra, P., Shim, Y.-B., 2012. Anal. Chem. 85, 1058–1064.
Zhou, Q., Lin, Y., Zhang, K., Li, M., Tang, D., 2018. Biosens. Bioelectron. 101, 146–152.